



Conditions for obtaining positronium Bose–Einstein condensation in a micron-sized cavity

Marcus X. Asaro^{1,a}, Steven Herrera², Melina Fuentes-Garcia¹, Gabriel G. Cecchini¹,
Erick E. Membreno¹, Rod G. Greaves¹, and Allen P. Mills Jr.^{1,b}

¹ Department of Physics and Astronomy, University of California, Riverside, CA 92521, USA

² Materials Science and Engineering Program, University of California, Riverside, CA 92521, USA

Received 7 March 2022 / Accepted 26 May 2022
© The Author(s) 2022, corrected publication 2022

Abstract. The quest for making a triplet positronium (Ps) Bose–Einstein condensate confined in a micron-sized cavity in a material such as porous silica faces at least three interrelated problems: (1) About 10^7 spin polarized Ps atoms must be injected into a small cavity within a porous solid material without vaporizing it. (2) It is known that Ps atoms confined in 30–100 nm diameter cavities in porous silica do not remain in the gas phase, but become stuck to the cavity walls at room temperature (Cooper et al., Phys. Rev. B 97:205302, 2018). (3) Cooling a gas of Ps atoms to cryogenic temperatures by energy exchange with the walls would be a very slow process (Saito and Hyodo, in: Surko, Gianturco (eds) New Directions in Antimatter Chemistry and Physics, Springer Dordrecht, Netherlands, 2001) because of the relatively low collision rate with the walls and the large mismatch between the masses of the Ps and the wall atoms. A possible solution of these difficulties is presented, based on cooling the implanted positrons in an isotopically pure diamond single crystal target, subsequent saturating of the wall Ps coverage so that a substantial portion of the Ps will be in the gaseous state, and thermalizing the gas-phase Ps via collisions with the low effective mass wall Ps. A design process for the target material is outlined as well, including preliminary results in porous cavity fabrication using focused ion beam milling.

1 Introduction

Positronium (Ps) is the hydrogen-like bound state of an electron and its positron antiparticle [1, 2]. The ground state of Ps is split into (1) a singlet with a mean lifetime of 125 ps that decays into two 511 keV photons; and (2) a triplet state with a mean lifetime of 142 ns that decays into three photons with total energy of 1022 keV [3, 4]. One of the most interesting possibilities with dense Ps is observing the first Bose–Einstein condensate (BEC) consisting of an atom that is its own antiparticle, by producing a large number of atoms in a small volume at or below a critical temperature [5–8]. Some designs for such an experiment have been based on the idea of depositing a large number of Ps atoms inside a cavity formed within a porous insulating material like silica (SiO_2) or possibly liquid ^4He bubbles containing many positrons [9]. One severe problem with these ideas is that having enough Ps atoms requires implanting a large number of energetic positrons in

small volume which can heavily distort the microstructure of the material, i.e. melt the solid target. A second problem is that the cooling time of the Ps is proportional to the effective mass of the atoms in the cavity walls times the mean free path of the Ps in the cavity, and it would be difficult to obtain a below room temperature gas in a 100 nm diameter cavity within one mean lifetime [10] without laser cooling [7, 11, 12]. Another main concern is the recent report of Cooper et al. [13] that Ps atoms inside such a cavity will likely become stuck to the inner walls of the cavity at room temperature and therefore might not be able to form a Boltzmann gas, let alone a BEC, in the vacuum space of the cavity.

The experimental work leading up to this conclusion began with Deutsch's discovery of positronium in 1951 [14] and Paulin and Ambrosino's discovery in 1968 that nearly free Ps is formed efficiently when fast beta-decay positrons are implanted into various fine ceramic powders [15]. Curry and Schawlow then showed that Ps is emitted into vacuum from a layer of MgO powder with a mean kinetic energy of 0.28 ± 0.10 eV [16]. Sferlazzo et al. then found that Ps appears to exist as a physisorbed surface state on a single crystal quartz surface at low temperatures, from which it can be desorbed into the vacuum with an activation energy of about 0.15 eV [17, 18]. On the other hand, Ps in nanoporous silica with a 2.7 nm mean pore diameter moves about

Contribution to the Topical Issue “Atomic, Molecular and Optical Techniques for Fundamental Physics”, edited by David Cassidy, Jesús Pérez Ríos, Randolph Pohl and Mingsheng Zhan.

^a e-mail: masar001@ucr.edu (corresponding author)

^b e-mail: apmjr@ucr.edu (corresponding author)

as a nearly free particle and cools to near room temperature (42 ± 3 meV) [19]. In apparent contradiction to this, it has been shown [13] that Ps in nanoporous silica containing isolated voids with diameters up to 75 nm is not free to move about and decays with a lifetime of 90 ns with no dependence on the average pore size above some critical size. From this it may be concluded that the Ps in large pores is attracted to the walls and might possibly move about along the inner wall surface, but is not emitted into the vacuum space at room temperature, whereas the Ps in a small pore has sufficient confinement energy to allow it to tunnel from pore to pore. All of these observations are in agreement with a calculation by Saniz et al. [20] which shows there is a Ps bound state at a flat quartz surface with a binding energy of 0.14 eV.

At first sight, the discovery of Cooper et al. [13] makes it seem hopeless to think of making a Ps BEC within a cavity because the Ps would stick on the inner surface of the cavity. However, there is a limit to the monolayer Ps density on the inner wall surface so that there will be a gaseous Ps component given a sufficient number of atoms. A serendipitous consequence of this situation is that the gas-phase Ps should cool rapidly [10] because the surface Ps is relatively strongly coupled to the wall phonons and rapidly comes to thermal equilibrium with the wall, and the volume Ps is quickly exchanging its energy with a surface Ps layer that has a very low effective mass compared to that of the wall phonons.

2 Saturating the wall coverage

We can obtain an estimate of the monolayer Ps surface density on a smooth cavity surface using Schick's two-dimensional hard core Boson model [21, 22]. The 100% polarized $m = 1$ triplet Ps–Ps scattering length at zero energy is [23] $a = 3.00a_0$, where a_0 is the Bohr radius of hydrogen, $a_0 = 0.0529$ nm. For a two-dimensional system the mean-field total energy per particle due to particle–particle repulsion at low surface densities n_{2D} is

$$\begin{aligned} \frac{E_{MF}}{N} &= \frac{2\pi\hbar^2 n}{m} \left| \frac{1}{\ln n_{2D} a^2} \right| \\ &= 0.239 \text{ eV} \times \frac{n_{2D}}{|\ln(0.0252n_{2D})|} \end{aligned} \quad (1)$$

Here n_{2D} is in units of nm^{-2} in the last expression, and the mass m is that of Ps, $2m_e$. The relation between E_{MF}/N and n_{2D} , displayed in Fig. 1, suggests that a Ps surface binding energy of about 0.14 eV [20] would support a surface density of pure $m = 1$ Ps equal to 1.5 nm^{-2} , thus ensuring that atoms in excess of this density would be in the gaseous state. For a $1 \mu\text{m}$ diameter cylindrical cavity 100 nm thick, the saturation number of $m = 1$ Ps atoms on the surfaces would be about 3×10^6 atoms, with the other three spin states,

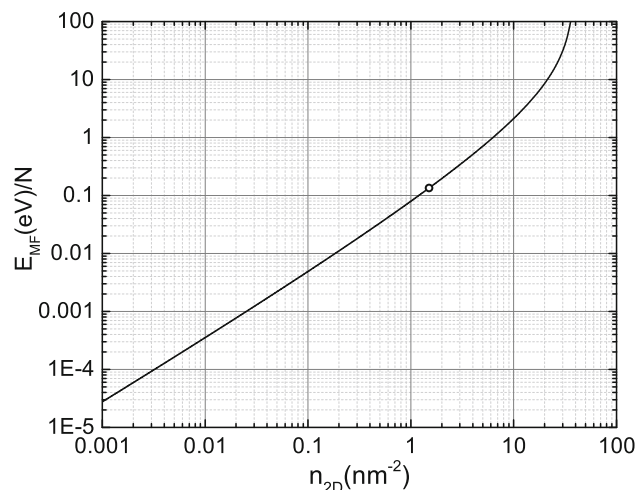


Fig. 1 Energy per atom in the mean-field approximation for a 2D distribution of spin-aligned triplet Ps atoms with surface density n_{2D} . The point on the curve represents the surface density at which the mean-field energy would be equal to the 0.14 eV surface binding energy of Ps on quartz [20]

including the singlets, having quickly annihilated. With an equal number of $m = 1$ atoms in the $0.079 \mu\text{m}^3$ volume of the cavity, the total $m = 1$ Ps number would be 6×10^6 , and the density in the gas phase would be $4 \times 10^{19} \text{ cm}^{-3}$ for which the BEC critical temperature would be about 170 K. In a more realistic model, the roughness of the cavity walls might affect the average surface density depending on the length scale of the roughness.

3 Obtaining high positronium densities

To achieve the BEC critical temperature of around 170 K, the total number of initial $m = 1$ Ps atoms will have to be double the foregoing maximum number, or 1.2×10^7 atoms, if we are using an incoming cylindrically symmetric Gaussian beam with a $1 \mu\text{m}$ FWHM. The initial number of incoming positrons will also need to be increased by a further factor of 10 because the fraction of positrons converted to Ps in the cavity is only about 40%, and because only approximately one-fourth of these will survive as pure triplet $m = 1$ atoms assuming the initial positron polarization is 50%. This value has been achieved by Rich et al. [24] by attenuating ^{22}Na beta-decay positrons by a factor of 4 or 5, reducing the number of slower and therefore less polarized positrons being moderated. The required initial peak positron areal density implanted at an energy of 5 keV into the $1 \mu\text{m}$ diameter central area of the target is about 200 times greater than the threshold instantaneous 2D density of 5 keV positrons that will melt a 150 nm thick Ni foil, and the resulting high temperatures would be completely incompatible with a low temperature BEC for any ordinary materials. How-

ever, the energy might be conducted away via ballistic phonons [25–27]¹ in an isotopically pure diamond target at a temperature of about 10 K and via the high thermal conductivity in regions where the temperature might be much greater.

3.1 Polarized positrons

At the high densities needed for making a Ps BEC a collection of Ps will quickly annihilate unless the positrons are partially polarized. 100% polarized positrons (polarization $p = 1$, or probability 1 of having their spins aligned parallel to the axis of quantization, i.e. the z -axis) combining with an equal number of unpolarized electrons produce a population of ground state Ps atoms with the following proportions in the four ground state sublevels:

$$\begin{aligned} 50\% \ ^3S_1 \ m = 1, \\ 25\% \ ^3S_1 \ m = 0, \quad \text{and} \\ 25\% \ ^1S_0 \ m = 0. \end{aligned} \tag{2}$$

The positron polarization is defined as $p = (N_{\uparrow} - N_{\downarrow}) / (N_{\uparrow} + N_{\downarrow})$, where N_{\uparrow} and N_{\downarrow} are the number of positrons having their spins aligned parallel or antiparallel to the z -axis. Positrons with polarization $0 < p < 1$ have probability $\frac{1}{2}(1 + p)$ of having their spins aligned parallel to the z -axis and $\frac{1}{2}(1 - p)$ of being antiparallel. Upon combining with unpolarized electrons to make ground state Ps, the probabilities of the four Ps states will be

$$\begin{aligned} \frac{1}{4}(1 + p) \ ^3S_1 \ m = 1, \\ \frac{1}{8}(1 + p) \ ^3S_1 \ m = 0, \\ \frac{1}{8}(1 + p) \ ^1S_0 \ m = 0 \end{aligned} \tag{3}$$

plus

$$\begin{aligned} \frac{1}{4}(1 - p) \ ^3S_1 \ m = -1, \\ \frac{1}{8}(1 - p) \ ^3S_1 \ m = 0, \\ \frac{1}{8}(1 - p) \ ^1S_0 \ m = 0 \end{aligned} \tag{4}$$

¹ The remarkably high thermal conductivity of diamond might possibly be compromised in an experiment by the ionization produced by the implanted positrons. Each 5 keV positron will produce an electron-hole (eh) pair for every ~ 30 eV of energy lost, or about 170 pairs per positron. The maximum number of eh pairs per unit volume in the initial volume occupied by the stopped positrons is 8.5×10^{16} eh pairs per cm^3 in a density of C atoms equal to $1.76 \times 10^{23} \text{ cm}^3$, amounting to 4.8×10^{-7} eh pairs per carbon atom, about three orders of magnitude less than the critical electron-hole liquid density in diamond. See Refs. [28–30].

for a total of

$$\begin{aligned} \frac{1}{4}(1 + p) \ ^3S_1 \ m = 1, \\ \frac{1}{4}(1 - p) \ ^3S_1 \ m = -1, \\ \frac{1}{4} \ ^3S_1 \ m = 0, \\ \frac{1}{4} \ ^1S_0 \ m = 0 \end{aligned} \tag{5}$$

At high densities the $^3S_1 \ m = -1$ atoms will spin exchange or form Ps_2 molecules with an equal number of $^3S_1 \ m = 1$ atoms, the $^3S_1 \ m = 0$ atoms will annihilate with each other, and the $^1S_0 \ m = 0$ atoms will have annihilated with their 125 ps lifetime. The probability P of the Ps being in an $m = 1$ state at high densities is then

$$P(^3S_1 \ m = 1) = \frac{1}{4}(1 + p) - \frac{1}{4}(1 - p) = \frac{1}{2}p. \tag{6}$$

It is then imperative that the positron polarization be made as large as possible [28]. An ordinary positron beam using a ^{22}Na positron source and a conical solid Ne moderator yields a beam of 28% polarized positrons [28]. We can get about 50% polarization by attenuating the fast positrons with a layer of absorbent material, such as Ar frozen over the source, that cuts the beam intensity to 25% [24] at the primary moderator. With this polarization, at most 25% of the positrons could form polarized Ps suitable for making a BEC.²

3.2 Dense positron production

The necessary high areal density of low energy positrons may in principle be achieved using the method of “brightness enhancement” [31]. In the present case this could be implemented as follows.

Positrons from a Penning–Surko buffer gas trap [32] are transported to a high-vacuum positron trap until about 6×10^8 positrons are collected and compressed using the rotating wall technique [33]. The positron plasma is ejected from the trap, accelerated to 5 keV, extracted from the guiding magnetic field, and focused

² A second choice that is much more difficult and uncertain would be to filter high density positrons through a layer of surface positrons on a remoderator foil that have made themselves 100% positively polarized by forming Ps_2 molecules. The remaining positively polarized surface positrons will not capture positively reemitted positrons but will capture negatively polarized positrons to make Ps_2 molecules, leaving only 100% polarized positron to be reemitted. In either case, the remoderated positrons will not be highly polarized if the remoderator foil is ferromagnetic with in-plane directions of the electron polarization, as would be the case with Ni below its Curie temperature, 354°C [29]. Non-ferromagnetic remoderators could be Al, W, Pt, Cu, etc. (e.g. Mills [30]).

by means of a magnetic lens to a $65\ \mu\text{m}$ FWHM diameter spot onto a $150\ \text{nm}$ [34] thick single crystal Ni(100) remoderator foil, making use of improvements to magnetic field extraction, as detailed by Hurst et al. [35]. The foil may be held above the $627\ \text{K}$ Curie temperature to prevent possible depolarization of the positron spins. Other moderators, such as Pt, W, and diamond, are possible that would have a good slow positron yield, but would not have to be heated. The positron pulse length can be extended from $3\ \text{ns}$ to approximately $50\ \text{ns}$ to minimize space charge effects upon focusing onto, and extraction from, the Ni foil.

The Ni has a negative affinity [36–38] for positrons, of which about 20% will be emitted from the backside of the foil and into the vacuum, with a kinetic energy of $1.1\ \text{eV}$ and a thermal energy spread dictated by the temperature of the remoderator foil, and an angular spread of about $\pm 0.2\ \text{rad}$ [34].

3.3 Remoderated positron implantation

The remoderated positrons are accelerated to $5\ \text{keV}$ and focused to less than $1\ \mu\text{m}$ FWHM onto a diamond target, shown in Fig. 2. The positrons stop in the diamond at a place that has been thinned to about $400\ \text{nm}$ thickness, reducing the potential number of useful $m = 1$ Ps atoms to about 6×10^7 . With a Ps cavity $1\ \mu\text{m}$ diameter $\times 0.1\ \mu\text{m}$ deep, and an initial positron spin-polarization of about 50%, the initial $m = 1$ triplet Ps density from Eq. (6), including a further 50% loss to wall Ps, will be about $4 \times 10^{19}\ \text{cm}^{-3}$, where the BEC critical temperature is around $170\ \text{K}$, as calculated in Sect. 2.

3.4 Heat transport

The central deposited energy per unit area ($7\ \text{J}\cdot\text{cm}^{-2}$), spread over a time of $50\ \text{ns}$ to reduce space charge effects, is removed via ballistic phonons in the diamond target and possibly assisted by the high thermal conductivity (see Fig. 2 of Ref. [40]) which is greater than $400\ \text{W}\cdot\text{cm}^{-1}\text{K}^{-1}$ between 50 and $100\ \text{K}$. The thermal diffusivity

$$\alpha = \frac{k}{\rho c_p}, \quad (7)$$

is the diffusion coefficient in the thermal diffusion equation

$$\frac{\partial T}{\partial t} = \alpha \nabla^2 T. \quad (8)$$

Here $k = (4 - 6) \times 10^4\ \text{W}\cdot\text{m}^{-1}\text{K}^{-1}$ is the range of the thermal conductivity of isotopically pure diamond between 50 and $100\ \text{K}$, and $\rho = 3.51 \times 10^3\ \text{kg}\ \text{m}^{-3}$ is the density of diamond. The specific heat of diamond at $100\ \text{K}$ is $c_p = 22.2\ \text{J}\cdot\text{kg}^{-1}\text{K}^{-1}$, and it varies between $(3.33 - 22.2)\ \text{J}\cdot\text{kg}^{-1}\text{K}^{-1}$ as T^3 between 50 and $100\ \text{K}$ [41]. Taking the thermal diffusivity at $100\ \text{K}$ to

be $\alpha = 0.513\ \text{m}^2\text{s}^{-1}$, the thermal diffusion length λ in a time $\tau = 10\ \text{ns}$ is

$$\lambda = \sqrt{\alpha\tau} = \sqrt{0.513\ \text{m}^2\text{s}^{-1} \times 10^{-8}\ \text{s}} = 71.6\ \mu\text{m}. \quad (9)$$

At $50\ \text{K}$, the diffusion length will be $\sqrt{8}$ times longer, or $203\ \mu\text{m}$ since the specific heat is following the Einstein–Debye T^3 dependence at low temperatures [42].

Since the phonon diffusion length will be 400 times larger than the radius r of the positron spot and 1600 times greater than the $130\ \text{nm}$ median penetration depth [43] of $5\ \text{keV}$ positrons in diamond, the volume of material in which the positron deposition energy will be eventually deposited will be greater by a factor of about $400^2 \times 1600 = 2.5 \times 10^8$ than the initial deposition volume, leading to a negligible temperature rise of only a few K. However, a complication arises as the roughly 100 times more numerous electron–hole pairs generated by the impinging $5\ \text{keV}$ positrons will scatter the ballistic phonons. The severity of this effect has been determined for pure Si at room temperature [44–46], but we know of no information about scattering of phonons from electron–hole pairs in diamond at low temperatures.

3.5 Positron mobility in diamond

The positron mobility in natural type IIa diamond (see Fig. 1 of Ref. [47]) at temperatures from 30 to $120\ \text{K}$ is $\mu \approx 250\ \text{cm}^2\text{V}^{-1}\text{s}^{-1}$. The positron diffusion coefficient at $100\ \text{K}$ in natural type IIa diamond is therefore $D = \mu kT/e = 2.5\ \text{cm}^2\text{s}^{-1}$, and the diffusion length in one mean positron lifetime, $\tau = (97.5 \pm 1.5)\ \text{ps}$ [48], is $\lambda = \sqrt{D\tau} \approx 0.16\ \mu\text{m}$. In isotopically pure CVD diamond the dip in the mobility that is observed at $150\ \text{K}$ in type IIa natural diamond would likely not be present, and the mobility should be proportional to $T^{-3/2}$, suggesting that at $30\ \text{K}$ the mobility could be $\mu = 4000\ \text{cm}^2\text{V}^{-1}\text{s}^{-1}$, with a diffusion length $\lambda \approx 1.76\ \mu\text{m}$. Thus, the positrons should efficiently reach the hollow cavity depicted in Fig. 2b and fill it with Ps [49, 50].

3.6 Emission of positronium at the diamond surface

Some of the positrons will be directly emitted into the cavity as Ps. The energetics of this process are quite well known for clean, hydrogen-free, (2×1) LEED-pattern type IIa diamond (100) surfaces, where at room temperature the positron work function is $-4.20 \pm 0.04\ \text{eV}$ [51]. On the other hand, the electron affinity—the minimum energy required to remove one electron from the valence band maximum to the vacuum for clean C(100) (2×1) —is $5.6\ \text{eV}$ [52]. Therefore the maximum energy of Ps emitted from these surfaces starting from a positron in its ground state and diamond with no excitations is $\phi_{\text{Ps}} = 4.2 + 6.8 - 5.6 = 5.4\ \text{eV}$. The fact that [39] the zero-energy extrapolated positron reemission probability at room temperature is 67% implies that 33% of the positrons escaping from diamond should be making free

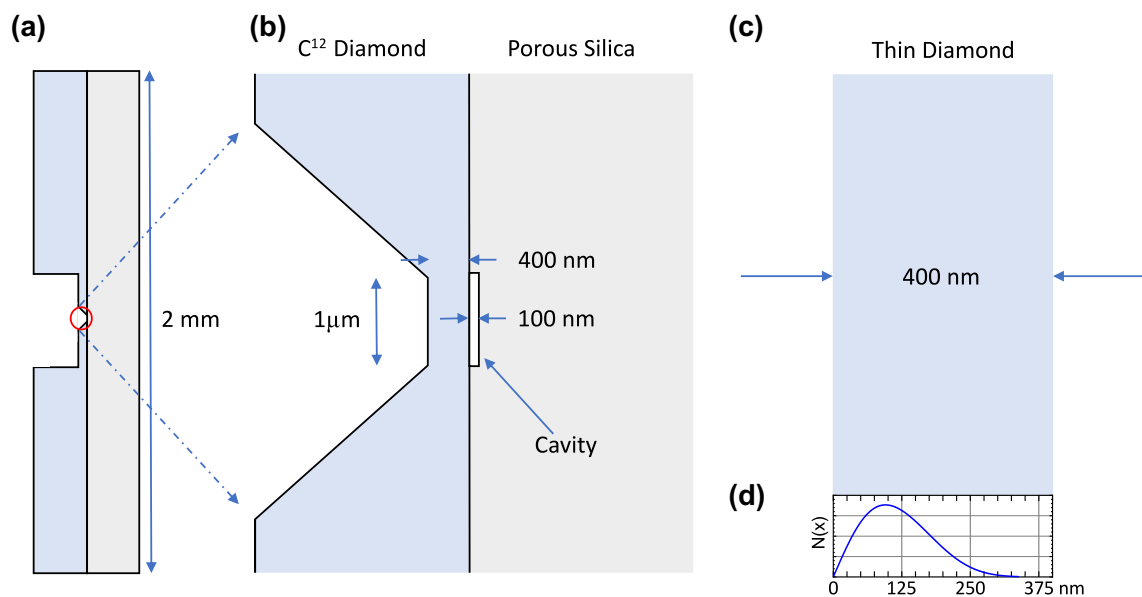


Fig. 2 Cross section of a possible isotopically pure diamond/porous silica target (a), with a close-up (b) of the 100 nm thick porous silica Ps cavity. Part (c) shows a magnified view of the thin (400 nm) diamond membrane and the graph in part (d) shows the stopping profile of 5 keV positrons in the thin diamond. The diamond surface facing the cavity would perhaps best be a hydrogen-terminated surface as discussed in Ref. [39], although carbinol-termination may be required if a stronger bond is needed

vacuum Ps. Some of the Ps or positrons may be stuck to the diamond surface as well as the porous silica surface, and some fraction of the energetic free positrons from the diamond could also make Ps via collisions with the silica.

We conclude that a sizable fraction of the positrons that escape into the cavity will make Ps and that it should be possible to produce a high density collection of cold polarized triplet Ps that would form a BEC with a critical temperature of about 170 K. The presence of such a BEC would be identified by measuring the angular correlation of annihilation radiation with an angular resolution of 0.1 mrad [53].

4 BEC target fabrication process

The fabrication of the BEC target will entail three distinct processes and result in an etched diamond window sharing a common surface with a cylindrically shaped cavity in a porous silica layer [54].

4.1 Fabrication of the porous silica cavity

In preliminary investigations various silica films were deposited on Si substrates using a magnetron sputtering system (AJA ORION 5) and RF power supply with discharge power of 300 W. The resulting film thickness was 300 nm. The deposition was performed at an Argon pressure of 11.25 mTorr, which would correspond to pore diameter sizes of 5.2 nm [54]. We chose sputter-

deposition of silicon dioxide over the sol-gel method [55] because of the controllability of the film thickness and porosity, as well as ease of use and quick turnover.

A gallium focused ion beam (FIB) incident on the film's surface was then used to mill a 1 μm diameter cavity (trench) to a depth of 100 nm (Fig. 3). For the initial attempts at milling porous silica, the Duobeam Quanta 200i FIB was used at 30 keV and 10 pA. With these parameters we were able to achieve cavity dimensions close to the target value in Sect. 2. An Asylum Research MFP-3D atomic force microscope (AFM) was used in AC mode with a 7 nm radius Si probe to analyze the topography of the sample. Depth profiles were taken along the x and y axes, as well as the diagonals, scanning left to right in the horizontal direction, to confirm the 100 nm depth and symmetry of the cavity. Note that it does appear that a slight pileup occurred in the lower left portion of the cavity interior according to the AFM image in (Fig. 3) and the bottom profile in green. There was also a 20 nm addition to the rim height in the upper portion of the cavity. Reducing the beam current should minimize this redeposition for future milling. Surface roughness of the surrounding area measuring 100 μm^2 was 3.3 nm.

To mitigate Ga^+ contamination and artifacts in the silica, following the milling operation a broad argon beam etch will be used to remove layers commensurate with the ion implantation depth. If Ga^+ contamination persists, as an alternative, a neon FIB may be used, which will remove the concern for such ion implantation while maintaining an acceptable sputter rate [56].

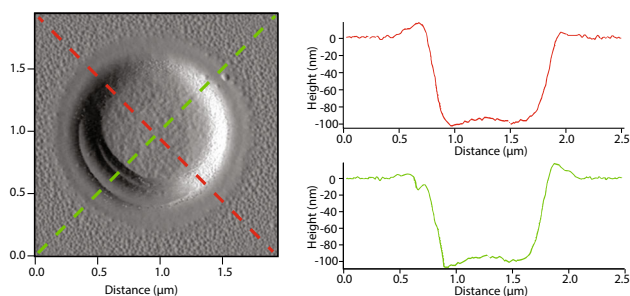


Fig. 3 AFM micrograph of the milled cavity in porous silica, with distances in microns. Dashed lines correspond to the orientation of the red and green depth (height) profiles, rastering from left to right on the micrograph

4.2 Etching of the diamond sample

The diamond to be used is an isotopically pure CVD diamond (100) with a thickness of 0.1 mm on a 1 mm ordinary CVD diamond substrate. A centrally located trench will be etched at the top face of the diamond using a process involving a reaction between Ni and diamond [57]

First, a $1541\ \mu\text{m} \times 1541\ \mu\text{m}$ Ni film will be deposited at the center of the diamond's top face. Then, the etching will occur via thermochemical reaction between the Ni film and diamond as it is annealed at $1000\ ^\circ\text{C}$ in water vapor for around 126 min (assuming an etch rate of $8.7\ \mu\text{m}/\text{min}$ [57]). After this process, the deposited film and oxide layers will be removed in a hot acid bath, leaving a truncated pyramidal trench in the diamond with the desired $1\ \mu\text{m} \times 1\ \mu\text{m}$ area and 400 nm thickness depicted in Fig. 2b.

4.3 Bonding of the silica and diamond sample

To complete the Ps BEC target, the diamond must be joined to the milled silica surface. By using a hydrogen-terminated diamond surface there may be some concern as to whether an adequate bond will form. In the case where a stronger bond is required, recent results [58] have shown that a diamond (100) carbinol-terminated surface can achieve a low-temperature direct bond to a silica substrate. Although this bonding process should be adequate to prevent slippage of the diamond surface facing the porous silica cavity, the Ps emission characteristics at the carbinol-terminated surface, as well as the question of Ps sticking to it, are not well understood at this time, and would require further investigation to determine it as a viable option.

Physical alignment of the micro-sized cavity with the identically sized diamond trench will be challenging. To resolve this issue, a flip chip bonder will be employed to achieve highly accurate alignment when bonding the two surfaces.

5 Conclusion

Previous research has shown that the Ps cooling rate in a porous silica cavity is very slow [10] and that the Ps will stick to the walls of the cavity, possibly preventing a dense Ps gas from forming a BEC. We have proposed that the Ps will cover the walls with a definite number of Ps per unit area owing to particle–particle repulsion, and atoms past this monolayer will be rapidly cooled, thereby populating the gas phase. Given this outlook, we presented a procedure for positron remoderation in which $\sim 10^8$ positrons are implanted into isotopically pure diamond and subsequently cooled via ballistic phonon emission. This would be followed by the saturation of the volume and surface of a milled cylindrical cavity by Ps. Such a scenario may achieve the low temperatures and volume densities for the realization of a Ps BEC.

Acknowledgements The authors are grateful to Prof. David B. Cassidy for comments. This work was supported in part by the US National Science foundation under Grant Nos. PHY 1807054, 2011836, and 2110626.

Author contributions

M.X. Asaro conceived the materials design and sample fabrication process, and assisted in the preparation of the manuscript. S. Herrera assisted in sample fabrication and characterization. M. Fuentes-Garcia assisted in the preparation of the manuscript and sample fabrication. G.G. Cecchini assisted in the preparation of the manuscript and discussion of the remoderated positron implantation. E.E. Membreno assisted in the preparation of the manuscript. R.G. Greaves contributed to the discussion of the remoderated positron implantation. A.P. Mills, Jr. developed the initial concept of the paper.

Data availability The datasets generated in this study are available from the corresponding author, A.P. Mills Jr., upon reasonable request.

Declarations

Conflict of interest The authors have no relevant financial or non-financial interests to disclose.

Open Access This article is licensed under a Creative Commons Attribution 4.0 International License, which permits use, sharing, adaptation, distribution and reproduction in any medium or format, as long as you give appropriate credit to the original author(s) and the source, provide a link to the Creative Commons licence, and indicate if changes were made. The images or other third party material in this article are included in the article's Creative Commons licence, unless indicated otherwise in a credit line to the material. If material is not included in the article's Creative Commons licence and your intended use is not permitted by statu-

tory regulation or exceeds the permitted use, you will need to obtain permission directly from the copyright holder. To view a copy of this licence, visit <http://creativecommons.org/licenses/by/4.0/>.

References

1. S. Berko, H.N. Pendleton, Positronium. *Annu. Rev. Nucl. Part. Sci.* **30**, 543 (1980). <https://doi.org/10.1146/annurev.ns.30.120180.002551>
2. A. Rich, Recent experimental advances in positronium research. *Rev. Mod. Phys.* **53**, 127 (1981). <https://doi.org/10.1103/RevModPhys.53.127>
3. D.B. Cassidy, Experimental progress in positronium laser physics. *Eur. Phys. J. D* **72**, 1 (2018). <https://doi.org/10.1140/epjd/e2018-80721-y>
4. P. Moskal, B. Jasińska, E.L. Stepień, S.D. Bass, Positronium in medicine and biology, *Nat. Rev. Phys.* **1**, 527 (2019). <https://doi.org/10.1038/s42254-019-0078-7>
5. P.M. Platzman, Surface positrons and the many positron, many electron system, in *Positron Studies of Solids, Surfaces, and Atoms*, ed. By S. Berko, A.P. Mills, W.S. Crane, K.F. Canter (World Scientific, Singapore, 1986), pp. 84–101, ISBN 997197844X. <https://books.google.com/books?id=0-DvAAAAAMAAJ>
6. A. Loeb, S. Eliezer, A gamma ray laser based on induced annihilation of electron–positron pairs. *Laser Part. Beams* **4**, 577 (1986). <https://doi.org/10.1017/S0263034600002263>
7. E.P. Liang, C.D. Dermer, Laser cooling of positronium. *Opt. Commun.* **65**, 419 (1988). [https://doi.org/10.1016/0030-4018\(88\)90116-2](https://doi.org/10.1016/0030-4018(88)90116-2)
8. P.M. Platzman, A.P. Mills Jr., Possibilities for Bose condensation of positronium. *Phys. Rev. B* **49**, 454 (1994). <https://doi.org/10.1103/PhysRevB.49.454>
9. A.P. Mills Jr., Positronium Bose–Einstein condensation in liquid ^4He bubbles. *Phys. Rev. A* **100**, 063615 (2019). <https://doi.org/10.1103/PhysRevA.100.063615>
10. H. Saito, T. Hyodo, Cooling and quenching of positronium in porous material, in *New Directions in Antimatter Chemistry and Physics*, ed. By C.M. Surko, F.A. Gianturco (Springer, Dordrecht, 2001), chap. 7, pp. 101–114, ISBN 9780792371526. https://link.springer.com/chapter/10.1007/0-306-47613-4_7
11. K. Shu, X. Fan, T. Yamazaki, T. Namba, S. Asai, K. Yoshioka, M. Kuwata-Gonokami, Study on cooling of positronium for Bose–Einstein condensation. *J. Phys. B: At. Mol. Opt.* **49**, 104001 (2016). <https://doi.org/10.1088/0953-4075/49/10/104001>
12. C. Zimmer, P. Yzombard, A. Camper, D. Comparat, Positronium laser cooling in a magnetic field. *Phys. Rev. A* **104**, 023106 (2021). <https://doi.org/10.1103/PhysRevA.104.023106>
13. B.S. Cooper, J.P. Boilot, C. Corbel, F. Guillemot, L. Gurung, L. Liskay, D.B. Cassidy, Annihilation of positronium atoms confined in mesoporous and macroporous SiO_2 films. *Phys. Rev. B* **97**, 205302 (2018). <https://doi.org/10.1103/PhysRevB.97.205302>
14. M. Deutsch, Evidence for the formation of positronium in gases. *Phys. Rev.* **82**, 455 (1951). <https://doi.org/10.1103/PhysRev.82.455>
15. R. Paulin, G. Ambrosino, Annihilation libre de l'orthopositonium formé dans certaines poudres de grande surface spécifique. *J. Phys. France* **29**, 263 (1968). <https://doi.org/10.1051/jphys:01968002904026300>
16. S.M. Curry, A.L. Schawlow, Measurements of the kinetic energy of free positronium formed in MgO . *Phys. Lett. A* **37**, 5 (1971). [https://doi.org/10.1016/0375-9601\(71\)90304-5](https://doi.org/10.1016/0375-9601(71)90304-5)
17. P. Sferlazzo, S. Berko, K.F. Canter, Experimental support for physisorbed positronium at the surface of quartz. *Phys. Rev. B* **32**, 6067 (1985). <https://doi.org/10.1103/PhysRevB.32.6067>
18. P. Sferlazzo, S. Berko, K.F. Canter, Time-of-flight spectroscopy of positronium emission from quartz and magnesium oxide. *Phys. Rev. B* **35**, 5315 (1987). <https://doi.org/10.1103/PhysRevB.35.5315>
19. D.B. Cassidy, P. Crivelli, T.H. Hisakado, L. Liskay, V.E. Meline, P. Perez, H.W.K. Tom, A.P. Mills Jr., Positronium cooling in porous silica measured via Doppler spectroscopy. *Phys. Rev. A* **81**, 012715 (2010). <https://doi.org/10.1103/PhysRevA.81.012715>
20. R. Saniz, B. Barbiellini, P.M. Platzman, A.J. Freeman, Physisorption of positronium on quartz surfaces. *Phys. Rev. Lett.* **99**, 096101 (2007). <https://doi.org/10.1103/PhysRevLett.99.096101>
21. M. Schick, Two-dimensional system of hard-core bosons. *Phys. Rev. A* **3**, 1067 (1971). <https://doi.org/10.1103/PhysRevA.3.1067>
22. G.E. Astrakharchik, J. Boronat, I.L. Kurbakov, Y.E. Lozovik, F. Mazzanti, Low-dimensional weakly interacting Bose gases: Nonuniversal equations of state. *Phys. Rev. A* **81**, 013612 (2010). <https://doi.org/10.1103/PhysRevA.81.013612>
23. I.A. Ivanov, J. Mitroy, K. Varga, Positronium-positronium scattering using the stochastic variational method. *Phys. Rev. A* **65**, 022704 (2002). <https://doi.org/10.1103/PhysRevA.65.022704>
24. A. Rich, R.S. Conti, D.W. Gidley, M. Skalsey, J. Vanhouse, P.W. Zitzewitz, Production and applications of monoenergetic polarized positron beams. *Hyperfine Interact.* **44**, 125 (1989). <https://doi.org/10.1007/BF02398663>
25. L. Brillouin, M. Parodi, *Wave Propagation in Periodic Structures*, 1st edn. (McGraw-Hill, New York, 1946)
26. R.J. von Gutfeld, A.H. Nethercot, Heat pulses in quartz and sapphire at low temperatures. *Phys. Rev. Lett.* **12**, 641 (1964). <https://doi.org/10.1103/PhysRevLett.12.641>
27. D. Huet, A. Zylbersztejn, J.P. Maneval, Measurement of acoustic-wave dispersion in solids. *Phys. Rev. Lett.* **29**, 1092 (1972). <https://doi.org/10.1103/PhysRevLett.29.1092>
28. D.B. Cassidy, V.E. Meline, A.P. Mills Jr., Production of a fully spin-polarized ensemble of positronium atoms. *Phys. Rev. Lett.* **104**, 173401 (2010). <https://doi.org/10.1103/PhysRevLett.104.173401>
29. B. Legendre, M. Sghaier, Curie temperature of nickel. *J. Therm. Anal. Calorim.* **105**, 141 (2011)
30. A.P. Mills Jr., Positron moderation and remoderation techniques for producing cold positron and positronium sources. *Hyperfine Interact.* **44**, 105 (1989)

31. A.P. Mills Jr., Brightness enhancement of slow positron beams. *Appl. Phys.* **23**, 189 (1980). <https://doi.org/10.1007/BF00899716>
32. R.G. Greaves, C.M. Surko, Inward transport and compression of a positron plasma by a rotating electric field. *Phys. Rev. Lett.* **85**, 1883 (2000). <https://doi.org/10.1103/PhysRevLett.85.1883>
33. J.R. Danielson, C.M. Surko, Torque-balanced high-density steady states of single-component plasmas. *Phys. Rev. Lett.* **94**, 035001 (2005). <https://doi.org/10.1103/PhysRevLett.94.035001>
34. P.J. Schultz, E.M. Gullikson, A.P. Mills Jr., Transmitted positron reemission from a thin single-crystal Ni(100) foil. *Phys. Rev. B* **34**, 442 (1986). <https://doi.org/10.1103/PhysRevB.34.442>
35. N.C. Hurst, J.R. Danielson, C.M. Surko, Magnetic field extraction of trap-based electron beams using a high-permeability grid. *Phys. Plasmas* **22**, 073503 (2015). <https://doi.org/10.1063/1.4923460>
36. D.G. Costello, D.E. Groce, D.F. Herring, J.W. McGowan, Evidence for the negative work function associated with positrons in gold. *Phys. Rev. B* **5**, 1433 (1972). <https://doi.org/10.1103/PhysRevB.5.1433>
37. B.Y. Tong, Negative work function of thermal positrons in metals. *Phys. Rev. B* **5**, 1436 (1972). <https://doi.org/10.1103/PhysRevB.5.1436>
38. S. Pendyala, D. Bartell, F.E. Girouard, J.W. McGowan, Energy distribution of slow positrons diffusing from incomplete *d*-shell transition metals. *Phys. Rev. Lett.* **33**, 1031 (1974). <https://doi.org/10.1103/PhysRevLett.33.1031>
39. G.R. Brandes, A.P. Mills, D.M. Zuckerman, Positron workfunction of diamond C(100) surfaces, in *Positron Annihilation—ICPA-9, Materials Science Forum* vol. 105–110, ed. by Z. Kajcsos, C. Szeles (Trans Tech Publ. Ltd., Switzerland, 1992), pp. 1363–1366. ISBN 087849636X. <https://www.scientific.net/MSF.105-110.1363>
40. L.H. Wei, P.K. Kuo, R.L. Thomas, T.R. Anthony, W.F. Banholzer, Thermal conductivity of isotopically modified single crystal diamond. *Phys. Rev. Lett.* **70**, 3764 (1993). <https://doi.org/10.1103/PhysRevLett.70.3764>
41. W. DeSorbo, Specific heat of diamond at low temperatures. *J. Chem. Phys.* **21**, 876 (1953). <https://doi.org/10.1063/1.1699050>
42. O.O. Vasil'ev, V.B. Muratov, T.I. Duda, The study of low-temperature heat capacity of diamond: Calculation and experiment. *J. Superhard Mater.* **32**, 375 (2010). <https://doi.org/10.3103/S106345761006002X>
43. A.P. Mills Jr., R.J. Wilson, Transmission of 1–6-keV positrons through thin metal films. *Phys. Rev. A* **26**, 490 (1982). <https://doi.org/10.1103/PhysRevA.26.490>
44. B. Liao, B. Qiu, J. Zhou, S. Huberman, K. Esfarjani, G. Chen, Significant reduction of lattice thermal conductivity by the electron-phonon interaction in silicon with high carrier concentrations: A first-principles study. *Phys. Rev. Lett.* **114**, 115901 (2015). <https://doi.org/10.1103/PhysRevLett.114.115901>
45. M. Dutta, S. Mandal, R. Hathwar, A.M. Fischer, F.A.M. Koeck, R.J. Nemanich, S.M. Goodnick, S. Chowdhury, Determination of minority carrier lifetime of holes in diamond p-i-n diodes using reverse recovery method. *IEEE Electr. Device Lett.* **39**, 552 (2018). <https://doi.org/10.1109/LED.2018.2804978>
46. J. Zhou, H.D. Shin, K. Chen, B. Song, R.A. Duncan, Q. Xu, A.A. Maznev, K.A. Nelson, G. Chen, Direct observation of large electron–phonon interaction effect on phonon heat transport. *Nat. Commun.* **11**, 6040 (2020). <https://doi.org/10.1038/s41467-020-19938-9>
47. A.P. Mills, G.R. Brandes, D.M. Zuckerman, W. Liu, S. Berko, Positron mobility in natural diamond, in *Positron Annihilation—ICPA-9, Materials Science Forum* vol 105–110 (Trans Tech Publ. Ltd., Switzerland, 1992), pp. 763–766, ISBN 087849636X. <https://www.scientific.net/MSF.105-110.763>
48. Y.S. Li, S. Berko, A.P. Mills, Positron lifetime in synthetic diamond, in *Positron Annihilation—ICPA-9, Materials Science Forum*, vol 105–110 (Trans Tech Publ. Ltd., Switzerland, 1992), pp. 739–742, ISBN 087849636X. <https://www.scientific.net/MSF.105-110.739>
49. K. Thonke, R. Schliesing, N. Teofilov, H. Zacharias, R. Sauer, A.M. Zaitsev, H. Kanda, T.R. Anthony, Electron-hole drops in synthetic diamond. *Diam. Relat. Mater.* **9**, 428 (2000). [https://doi.org/10.1016/S0925-9635\(99\)00315-5](https://doi.org/10.1016/S0925-9635(99)00315-5)
50. E.I. Lipatov, D.E. Genin, D. Grigor'ev, V.F. Tarasenko, Recombination radiation in the diamond, in *Luminescence—An Outlook on the Phenomena and their Applications*, ed. By J. Thirumalai (IntechOpen, London, 2016), chap. 9, pp. 191–224, ISBN 9789535127635. <https://doi.org/10.5772/65064>
51. G.R. Brandes, A.P. Mills Jr., Work function and affinity changes associated with the structure of hydrogen-terminated diamond (100) surfaces. *Phys. Rev. B* **58**, 4952 (1998). <https://doi.org/10.1103/PhysRevB.58.4952>
52. L. Diederich, O. Kuttel, P. Aebi, L. Schlapbach, Electron affinity and work function of differently oriented and doped diamond surfaces determined by photoelectron spectroscopy. *Surf. Sci.* **418**, 219 (1998). [https://doi.org/10.1016/S0039-6028\(98\)00718-3](https://doi.org/10.1016/S0039-6028(98)00718-3)
53. G.G. Cecchini, A.C.L. Jones, M. Fuentes-Garcia, D.J. Adams, M. Austin, E. Membreno, A.P. Mills Jr., Detector for positronium temperature measurements by two-photon angular correlation. *Rev. Sci. Instrum.* **89**, 053106 (2018). <https://doi.org/10.1063/1.5017724>
54. Y. Kobayashi, W. Zheng, T.B. Chang, K. Hirata, R. Suzuki, T. Ohdaira, K. Ito, Nanoporous structure of sputter-deposited silicon oxide films characterized by positronium annihilation spectroscopy. *J. Appl. Phys.* **91**, 1704 (2002). <https://doi.org/10.1063/1.1428787>
55. D. Zhao, J. Feng, Q. Huo, N. Melosh, G.H. Fredrickson, B.F. Chmelka, G.D. Stucky, Triblock copolymer syntheses of mesoporous silica with periodic 50 to 300 angstrom pores. *Science* **279**, 548 (1998). <https://doi.org/10.1126/science.279.5350.548>
56. K.T. Mahady, S. Tan, Y. Greenzweig, A. Raveh, P.D. Rack, Monte Carlo simulation of nanoscale material focused ion beam gas-assisted etching: Ga⁺ and Ne⁺ etching of SiO₂ in the presence of a XeF₂ precursor gas. *Nanoscale Adv.* **1**, 3584 (2019). <https://doi.org/10.1039/C9NA00390H>
57. M. Nagai, K. Nakanishi, H. Takahashi, H. Kato, T. Makino, S. Yamasaki, T. Matsumoto, T. Inokuma, N.

Tokuda, Anisotropic diamond etching through thermochemical reaction between Ni and diamond in high-temperature water vapour. *Sci. Rep.* **8**, 1 (2018). <https://doi.org/10.1038/s41598-018-25193-2>

58. T. Matsumae, Y. Kurashima, H. Takagi, H. Umezawa, E. Higurashi, Low-temperature direct bonding of diamond (100) substrate on Si wafer under atmospheric conditions. *Scr. Mater.* **191**, 52 (2021). <https://doi.org/10.1016/j.scriptamat.2020.09.006>